

Variational Quantum Algorithms for Trace Distance and Fidelity Estimation

Ranyiliu Chen,¹ Zhixin Song,¹ Xuanqiang Zhao,¹ and Xin Wang^{1,*}

¹*Institute for Quantum Computing, Baidu Research, Beijing 100193, China*

(Dated: September 7, 2021)

Estimating the difference between quantum data is crucial in quantum computing. However, as typical characterizations of quantum data similarity, the trace distance and quantum fidelity are believed to be exponentially-hard to evaluate in general. In this work, we introduce hybrid quantum-classical algorithms for these two distance measures on near-term quantum devices where no assumption of input state is required. First, we introduce the Variational Trace Distance Estimation (VTDE) algorithm. We in particular provide the technique to extract the desired spectrum information of any Hermitian matrix by local measurement. A novel variational algorithm for trace distance estimation is then derived from this technique, with the assistance of a single ancillary qubit. Notably, VTDE could avoid the barren plateau issue with logarithmic depth circuits due to a local cost function. Second, we introduce the Variational Fidelity Estimation (VFE) algorithm. We combine Uhlmann's theorem and the freedom in purification to translate the estimation task into an optimization problem over a unitary on an ancillary system with fixed purified inputs. We then provide a purification subroutine to complete the translation. Both algorithms are verified by numerical simulations and experimental implementations, exhibiting high accuracy for randomly generated mixed states.

I. INTRODUCTION

With surging advances in material, manufacturing, and quantum control, quantum computing has been driven into the noisy intermediate-scale quantum (NISQ) era [1], which requires novel algorithms running on a limited number of qubits with unwanted interference of the environment. The hybrid quantum-classical computation framework [2] is regarded as well-suited for execution on NISQ devices and is expected to show practical near-term applications in quantum chemistry and quantum machine learning [3–5]. Specifically, hybrid quantum-classical algorithms utilize the parameterized quantum circuits (PQCs) [6] and classical optimization to solve problems in many areas, including Hamiltonian ground and excited states preparation [7, 8], quantum compiling [9], Gibbs state preparation [10–13], and quantum linear algebra [14–18]. We refer to [19–21] for a detailed review.

Applications mentioned above and many other quantum information tasks suffer from unwanted interactions with the environment when implemented by real-world quantum systems, leading to errors in their working qubits. Thus, metric estimation for quantum states is vital to benchmark the tasks' implementation. As scalable quantum computers and quantum error correction are still on their way [22], estimating metric on a near-term device is essential to the verification of quantum information processing tasks and quantify how well quantum information has been preserved. Moreover, metric estimation is also an integral part of quantum machine learning [3–5]. For example, metrics could play the role of the loss function in state learning tasks [23, 24].

The trace distance and fidelity are two typical metrics to quantify how close two quantum states are [25–27]. Given two quantum states ρ and σ , the trace distance $D(\rho, \sigma)$ and

the fidelity $F(\rho, \sigma)$ are defined as follows:

$$D(\rho, \sigma) := \frac{1}{2} \|\rho - \sigma\|_1, \quad (1)$$

$$F(\rho, \sigma) := \text{Tr} \sqrt{\sqrt{\rho} \sigma \sqrt{\rho}} = \|\sqrt{\rho} \sqrt{\sigma}\|_1, \quad (2)$$

where $\|\cdot\|_1$ denotes the trace norm. When at least one of the states is pure, the task of fidelity estimation reduces to the simple case of calculating the square root of the state overlap $F(\rho, \sigma) = \sqrt{\text{Tr} \rho \sigma}$ which can be obtained by the Swap-test [28]. Thus the trace distance in this case is bounded by $1 - F(\rho, \sigma) \leq D(\rho, \sigma) \leq \sqrt{1 - F(\rho, \sigma)^2}$. However, evaluating these two metrics for mixed states is hard in general. One might attempt to classically compute the two metric from the matrix description of quantum states ρ and σ obtained via quantum state tomography. Nevertheless, this approach is infeasible due to the exponential growth of the matrix dimension with the number of qubits. On quantum computers, evaluating the trace distances is probably hard since even judging whether ρ and σ have large or small trace distance is known to be QSZK-complete [29], where QSZK (quantum statistical zero-knowledge) is a complexity class that includes BQP (bounded-error quantum polynomial time). Hence estimating fidelity and trace distance could probably be hard even for quantum computers.

Several approaches have been proposed for the trace distance and fidelity estimation, and here we focus on the case where the metric is between two unknown general quantum states. In [30], the authors variationally estimate the truncated fidelity via a hybrid classical-quantum algorithm. The truncated fidelity bounds the exact fidelity and is a good approximation of it when one of the states is known to have a low rank. For the estimation of trace distance, several methods are proposed but only applicable in specific quantum environments [31, 32]. To the best of our knowledge, no methods for estimating the trace distance on general NISQ devices has been proposed yet.

To overcome these challenges, we propose the Variational Trace Distance Estimation (VTDE) algorithm as well as the

*Electronic address: wangxin73@baidu.com

Variational Fidelity Estimation (VFE) algorithm. First, we propose a method to estimate the trace norm of an arbitrary Hermitian matrix H , and apply it to trace distance estimation by specifying $H = \frac{1}{2}(\rho - \sigma)$. In particular, we prove that local measurements on an ancillary single qubit can extract the desired spectrum information of any Hermitian H conjugated by a unitary. By optimizing over all unitaries, we can obtain the trace norm of H . Our method notably only employs a local observable in the loss function evaluation, which saves us from the gradient vanishing issue with shallow circuits. Second, we introduce a method to estimate the fidelity of general quantum states, which utilizes the Uhlmann's theorem. We observe that the fidelity can be estimated by optimizing over all unitaries on an ancillary system via the freedom in purification. We also introduce a subroutine that works on NISQ devices to purify quantum states. With the performance analysis of the purification subroutine, we show that only few ancillary qubits are required if the unknown states are low-rank.

This paper is organized as follows. In Sec. II, we introduce the variational quantum algorithms for trace norm and trace distance estimation. In Sec. III, we introduce the variational quantum algorithms for quantum state fidelity estimation and its purification subroutine for mixed state learning. Numerical experiments and experimental implementations on IMB superconducting device are provided to show the validity of our methods. We finally deliver concluding remarks in Sec. IV.

II. VARIATIONAL TRACE DISTANCE ESTIMATION

This section introduces a variational quantum algorithm for estimating the trace norm of an arbitrary Hermitian matrix H , which could be easily applied to trace distance estimation. Our method employs the optimization of a parameterized quantum circuit (PQC), requiring only one ancillary qubit initialized in an arbitrary pure state (typically $|0\rangle\langle 0|$ in practice) and single-qubit measurements. In this sense, our algorithm is practical and efficient for NISQ devices.

We will frequently use symbols such as \mathcal{H}_A and \mathcal{H}_B to denote Hilbert spaces associated with quantum systems A and B , respectively. We use d_A to denote the dimension of system A . The set of linear operators acting on A is denoted by $\mathcal{L}(\mathcal{H}_A)$. We usually write an operator with a subscript indicating the system that the operator acts on, such as M_{AB} , and write $M_A := \text{Tr}_B M_{AB}$. Note that for a linear operator $X \in \mathcal{L}(\mathcal{H}_A)$, we define $|X| = \sqrt{X^\dagger X}$, and the trace norm of X is given by $\|X\|_1 = \text{Tr}|X|$.

We first formulate the theory for the trace norm estimation, then we describe in detail the process of our algorithm, followed by the numerical experiments.

A. Estimating trace norm via one-qubit overlap maximization

Suppose on system $\mathcal{H}_A \otimes \mathcal{H}_B$ we have a Hermitian matrix H_{AB} that has spectral decomposition

$$H_{AB} = \sum_{j=1}^{d_A d_B} h_{AB}^j |\psi_j\rangle\langle\psi_j| \quad (3)$$

with decreasing spectrum $\{h_{AB}^j\}_{j=1}^{d_A d_B}$ and orthonormal basis $\{|\psi_j\rangle\}$. Here, for technical convenience, we simply pad the spectrum with 0s to ensure the expression in Eq. (3).

Before showing the main algorithm, we introduce an optimization method to obtain some information of the spectrum of a given Hermitian matrix as follows.

Proposition 1 *For any Hermitian matrix $H_{AB} \in \mathcal{L}(\mathcal{H}_A \otimes \mathcal{H}_B)$ with spectral decomposition as Eq. (3), respectively denote the dimension of \mathcal{H}_A , \mathcal{H}_B by d_A , d_B . It holds that*

$$\max_U \text{Tr} |0\rangle\langle 0|_A \tilde{H}_A = \sum_{j=1}^{d_B} h_{AB}^j, \quad (4)$$

where $\tilde{H}_A = \text{Tr}_B \tilde{H}_{AB}$, $\tilde{H}_{AB} = U H_{AB} U^\dagger$, and the optimization is over all unitaries.

This Proposition indicates that the optimization over unitaries can estimate the sum of several largest eigenvalues of H_{AB} . The proof of Proposition 1 can be found in Appendix IA.

To apply Proposition 1 to estimate the trace norm, we fix subsystem A to be single-qubit. In this case, for arbitrary Hermitian H_{AB} on $d = 2^n$ -dimensional quantum system $\mathcal{H}_A \otimes \mathcal{H}_B$, where $\mathcal{H}_A = \mathbb{C}^2$ (hence $\mathcal{H}_B = \mathbb{C}^{2^{n-1}}$), the maximal expectation of measurements on system A gives us the sum of the first half eigenvalues of H_{AB} . It is now quite close to the trace norm of H_{AB} , which is the sum of absolute values of its eigenvalues. We take the final step to estimate the trace norm by appending a 1-qubit pure state and optimizing twice. Concretely, we derive the following theorem to ensure the validity of our algorithm.

Theorem 2 *For any Hermitian H_A on n -qubit system A , and any single-qubit pure state $|r\rangle$ on system R , it holds that*

$$\|H_A\|_1 = \max_{U^+} \text{Tr} |0\rangle\langle 0|_R Q_R^+ + \max_{U^-} \text{Tr} |0\rangle\langle 0|_R Q_R^-, \quad (5)$$

where $Q_R^\pm = \text{Tr}_A Q_{AR}^\pm$, $Q_{AR}^\pm = U^\pm (\pm H_A \otimes |r\rangle\langle r|_R) U^{\pm\dagger}$, and each optimization is over unitaries on system AR .

This theorem shows how to generally evaluate the trace norm of arbitrary H by optimization. The proof of Theorem 2 can be found in Appendix 1B.

We note that, since the target Hermitian matrix is in many cases (and can always be) written as the linear combination of density matrix with real coefficients c^j :

$$H_A = \sum_j c^j \rho_A^j, \quad (6)$$

we have $\text{Tr } H_A = \sum_j c^j$. Employing the information of $\text{Tr } H_A$ we can save one optimization as the following Corollary shows:

Corollary 3 For any Hermitian H_A (written as Eq. (6)) on n -qubit system A , and any single-qubit pure state $|r\rangle$ on system R , it holds that

$$\begin{aligned} \|H_A\|_1 &= \sum_{h_A^j > 0} h_A^j + \sum_{h_A^j < 0} -h_A^j \\ &= 2 \sum_{h_A^j > 0} h_A^j - \text{Tr } H_A \\ &= 2 \max_U \text{Tr } |0\rangle\langle 0|_R Q_R - \sum_j c^j, \end{aligned} \quad (7)$$

where $Q_R = \text{Tr}_A Q_{AR}$, $Q_{AR} = U(H_A \otimes |r\rangle\langle r|_R)U^\dagger$, and the optimization is over all unitaries on system AR .

Also in this case, $\max_U \text{Tr } |0\rangle\langle 0|_R Q_R$ in practice can be evaluated by post-processing:

$$\text{Tr } |0\rangle\langle 0|_R Q_R = \sum_j c^j \text{Tr } |0\rangle\langle 0|_R (U\rho_A^j \otimes |r\rangle\langle r|_R U^\dagger)_R. \quad (8)$$

This means that we could use PQC, taking ρ_A^j as inputs, to perform the optimization for the trace norm estimation. In next section we will adopt this strategy to estimate the trace distance, for which $H = \frac{1}{2}(\rho - \sigma)$.

B. Variational trace distance estimation algorithm

Based on corollary 3, we are now ready to show our trace distance estimation (VTDE) algorithm for arbitrary quantum states ρ and σ . Fig. 1 demonstrates the diagram of our algorithm.

Specifically, with $H_A = \frac{1}{2}(\rho_A - \sigma_A)$ and $\text{Tr } H_A = 0$, Eq. (7) could be written as

$$\begin{aligned} D(\rho, \sigma) &= \frac{1}{2} \|\rho_A - \sigma_A\|_1 \\ &= \max_U (\text{Tr } |0\rangle\langle 0|_R \tilde{\rho}_R - \text{Tr } |0\rangle\langle 0|_R \tilde{\sigma}_R), \end{aligned} \quad (9)$$

where $\tilde{\rho}_{AR} = U(\rho_A \otimes |r\rangle\langle r|_R)U^\dagger$, $\rho_R = \text{Tr}_A \rho_{AR}$ and $\tilde{\sigma}_{AR} = U(\sigma_A \otimes |r\rangle\langle r|_R)U^\dagger$, $\sigma_R = \text{Tr}_A \sigma_{AR}$. This observation finally enables us to estimate the trace distance by optimization over unitaries, and the algorithm is given in Algorithm 1 in detail. In our VTDE algorithm, $\text{Tr } |0\rangle\langle 0|_R \tilde{\rho}_R$ and $\text{Tr } |0\rangle\langle 0|_R \tilde{\sigma}_R$ are evaluated successively, then the difference between them are maximized by a classical computer. In practice, the ancillary pure state can be initially set as $|r\rangle = |0\rangle$. We adopt a hardware efficient ansatz [33, 34] consisting of parameterized single-qubit R_y and R_z rotations, along with CNOT gates on adjacent qubits as entanglement gates (also see Fig. 1) to implement the tunable unitary evolution.

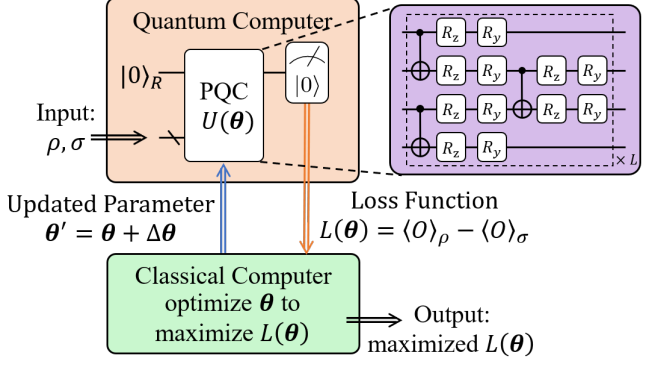


FIG. 1: Diagram of VTDE. VTDE employs a single-qubit ancilla for arbitrary number of qubits of ρ and σ . The outputs $\langle O \rangle_\rho$, $\langle O \rangle_\sigma$ are obtained by locally measuring the overlap with state $|0\rangle_R$. Then the optimization of the measurement outcome is undertaken by a classical computer (the green box). The unitary evolution on the coupled system is simulated by a hardware-efficient ansatz, of which the single qubit rotation gates (R_y , R_z) are controlled by classical parameters θ .

Algorithm 1 Variational Trace Distance Estimation (VTDE)

Input: quantum states ρ_A and σ_A , circuit ansatz of unitary $U_{AR}(\theta)$, number of iterations ITR;
Output: an estimate of trace distance $D(\rho_A, \sigma_A)$.
 Initialize parameters θ .
 Append ρ_A and σ_A with single-qubit state $|0\rangle_R$, respectively.
for $\text{itr} = 1, \dots, \text{ITR}$ **do**
 Apply $U_{AR}(\theta)$ to $\rho_A \otimes |0\rangle\langle 0|_R$ and $\sigma_A \otimes |0\rangle\langle 0|_R$, obtain the states $\tilde{\rho}_{AR} = U_{AR}(\theta)\rho_A \otimes |0\rangle\langle 0|_R U_{AR}(\theta)^\dagger$ and $\tilde{\sigma}_{AR} = U_{AR}(\theta)\sigma_A \otimes |0\rangle\langle 0|_R U_{AR}(\theta)^\dagger$, respectively.
 Evaluate $O_\rho = \text{Tr } |0\rangle\langle 0|_R \tilde{\rho}_R$ and $O_\sigma = \text{Tr } |0\rangle\langle 0|_R \tilde{\sigma}_R$ by measurement on system R .
 Compute the loss function $\mathcal{L}_1 := O_\rho - O_\sigma$.
 Maximize the loss function \mathcal{L}_1 and update parameters θ .
end for
 Output the optimized \mathcal{L}_1 as the trace distance estimate.

From Algorithm 1 one can tell that our VTDE estimates the trace distance for arbitrary quantum states without requiring any pre-knowledge. Furthermore, Algorithm 1 and Fig. 1 imply that VTDE employs a single-qubit ancillary qubit for any input size n of ρ and σ , and perform local (single-qubit) measurement in each iteration. In this sense, VTDE is general and efficient for NISQ devices. Recall that Algorithm 1 can be adapted to trace norm estimation for any H with decomposition $H = \sum_j c^j \rho^j$ based on Corollary 3.

Given the VTDE, we briefly discuss analytic gradient and the gradient vanishing (barren plateau [35]) issues. Analytic gradient enables us to perform gradient descent to optimize the parameters. As our VTDE employs an hardware-efficient PQC, the parameter shift rule [36, 37] is capable in our case to obtain analytic gradient. As for the barren plateau from which many variational quantum algorithms may suffer. We remark that our VTDE performs single-qubit measurements and takes the result as the loss function. This is essentially equivalent to a local observable, which has been proved to have at worst

a polynomially vanishing gradient with a shallow PQC [38]. In this sense, our VTDE could avoid the barren plateau issue when the number of layers $L \in \mathcal{O}(\log n)$.

We would like to remark that, the Naimark extension (see Example 2.2 of [39]) together with the property of trace distance that

$$D(\rho, \sigma) = \max_{0 \leq P \leq 1} \text{Tr} P(\rho - \sigma) \quad (10)$$

also explain VTDE. Indeed our idea is to study the capability of parameterized quantum circuits in extracting spectrum information from local measurements. Nevertheless, VTDE can be generalized for trace norm estimation of arbitrary H (Theorem 2 and Corollary 3), where trace norm estimation in Eq. (10) does not hold if we simply replace $(\rho - \sigma)$ by a non-traceless H . This generalization can be lead to wider applications in quantum information like the estimation of log negativity. Our intermediate product (Proposition 1) also indicates that the partial sum of the spectrum can be extracted by local measurements.

C. Numerical experiments

Numerical experiments are undertaken to demonstrate the validity and advantage of VTDE. All simulations including optimization loops are implemented via Paddle Quantum [40] on the PaddlePaddle Deep Learning Platform [41, 42].

We firstly estimate the trace distance between the 4-qubit GHZ state $|\psi\rangle = \frac{1}{\sqrt{2}}(|0000\rangle + |1111\rangle)$ and its output after the depolarizing channel:

$$\text{Dep}_p(\rho) = p \text{Tr} \rho \frac{I}{2^4} + (1-p)\rho. \quad (11)$$

In the experiment setting, we let $\rho = |\phi\rangle\langle\phi|$ and $\sigma = \text{Dep}_p(\rho)$, where the channel parameters are $p = \{0.1, 0.3, 0.5, 0.7, 0.9\}$. For the hyper-parameters, we set ITR = 120 and learning rate LR = 0.02. Fig. 2 shows the trace distance learned by VTDE versus the numbers of iterations. As one can see, for all considered channel parameters, the trace distance between ρ and σ can be estimated accurately within feasible iterations (< 120).

Next, we explore the required number of layers of the ansatz for input states with distinct ranks. Specifically, we set the number of qubits $n = 3$ and $\text{Rank}(\sigma) = 2$, while $\text{Rank}(\rho)$ ranges from 1 to $2^n = 8$. We randomly sample 100 states for each number of ranks of σ , and compute the accuracy for circuits with 1, 2 and 4 layers. Here the accuracy is defined as $\text{Acc.} = D_{\text{est}}/D_{\text{ide}}$, where $D_{\text{est}, \text{ide}}$ are the estimated and ideal trace distances, respectively. Hyper-parameters are the same as the previous experiment. Fig. 3 summarizes the result, telling that the behavior of a 4-layer circuit is more accurate and stable, while circuits with fewer layers perform badly and unstably for any rank of ρ , possibly due to the lack in expressibility [43].

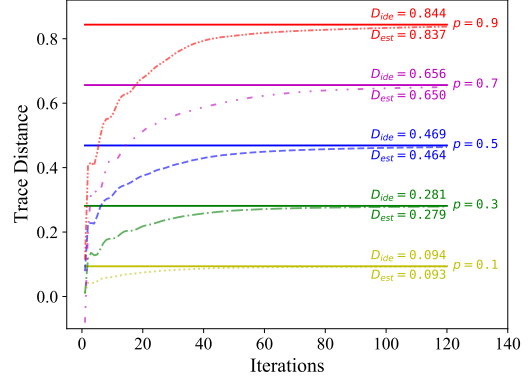


FIG. 2: Learning processes of VTDE, where the input states ρ and σ are 4-qubit GHZ state and its output after the depolarizing channel. The different colors correspond to considered depolarizing channel parameters $p = \{0.1, 0.3, 0.5, 0.7, 0.9\}$, with $p = 0.9$ being the top two red lines. We denote the ideal trace distances by D_{ide} and solid lines, and denote the estimated ones by D_{est} and dashed/dotted lines.

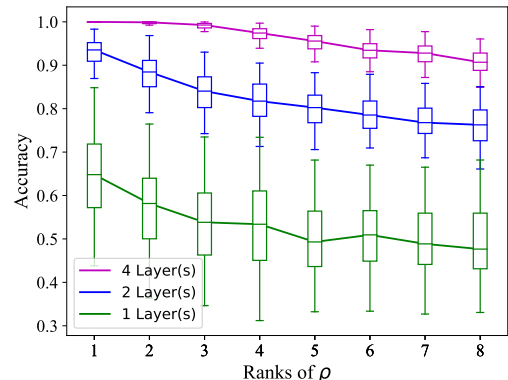


FIG. 3: Trace distance learned by VTDE with different number of layers versus the rank of ρ . The curves connect the median values in the boxplots displaying the distribution of the estimation of D between 100 sampled state pairs. Each curve corresponds to the 1-, 2-, or 4-layer case.

D. Implementation on superconducting quantum processor

We also apply our VTDE to estimate the trace distance between $|+\rangle$ state and itself affected by a dephasing channel:

$$\text{Deph}_p(\rho) = pZ\rho Z + (1-p)\rho. \quad (12)$$

The result with comparison to the values achieved from simulation are listed in Table I. The experiments are performed on the *IBM quantum* platform, loading the quantum device *ibmq_quito* containing 5 qubits.

The input state we choose here are $\rho = |+\rangle$ and $\sigma = \text{Deph}_{0.7}(\rho)$. On the quantum device, the input state σ is prepared by applying two *Ry* gates on the working and ancilla qubits with parameters $\pi/2$ and $2 \arcsin \sqrt{0.7} \approx 1.982$ respectively, followed by a *Control-Z* gate, then discarding the

Backends	mean	variance	error rate
Theoretical value	0.7	-	-
Simulator	0.70322	0.00010	0.46%
<i>ibmq_quito</i>	0.64312	0.00025	8.13%

TABLE I: Error analysis for VTDE between $\rho = |+\rangle$ and $\sigma = \text{Deph}_p(\rho)$. We choose $p = 0.7$ and repeat the experiment 10 times independently.

ancilla. Next, we operate parameterized quantum circuit on qubits, and use sequential minimal optimization [44] to optimize the parameters until the cost converge to its maximum. We repeat 10 independent experiments with same input states and randomly initialized parameters.

As demonstrated in Table I, the estimates converges stably for the simulator and the quantum device. Correspondingly, the achieved trace distance estimates by simulator (0.7032) is closer to the theoretical values (0.7) than that of quantum device (0.64312), which may caused by the quantum device noises.

III. VARIATIONAL FIDELITY ESTIMATION

In this section, we introduce Variational Fidelity Estimation (VFE) as a hybrid quantum-classical algorithm for estimating fidelity in the most general case where two mixed states are provided. The intuition of VFE lies in Uhlmann's theorem and the freedom in purification, based on which we prove that optimization over unitaries can obtain the fidelity. The purification of each quantum state is required by the optimization, for which we design a variational quantum state learning (VQSL) algorithm as the subroutine of our VFE. Both VFE and VQSL employs PQC to implement the optimization over unitaries. We give the theory behind and the process of VFE and VQSL, respectively, followed by numerical experiments. The diagram of VFE is shown in Fig. 4.

A. Theory and algorithm for fidelity estimation

Suppose we have two unknown quantum states, ρ_A and σ_A , on system A . With arbitrary purification of ρ_A and σ_A (denoted by $|\psi\rangle_{AR}$ and $|\phi\rangle_{AR}$, respectively), Corollary 6 allows us to estimate the fidelity of ρ_A and σ_A . As the prerequisite of Corollary 6, we first introduce Uhlmann's theorem and the freedom in purification:

Theorem 4 (Uhlmann's theorem, [25]) *Suppose ρ and σ are states of quantum system A . Then, for given quantum purification $|\psi\rangle_{AR}$ of ρ_A on system AR ,*

$$F(\rho_A, \sigma_A) = \max_{|\phi\rangle_{AR}} |\langle\psi|\phi\rangle_{AR}|, \quad (13)$$

where the maximization is over all purifications $|\phi\rangle_{AR}$ of σ_A on system AR .

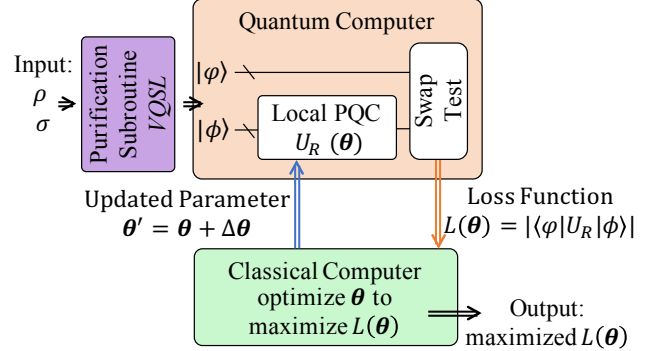


FIG. 4: Diagram of VFE. VFE employs a purification subroutine to purify ρ and σ . The outputs $\langle\psi|U_R|\phi\rangle$ are obtained by the swap test. Then the optimization of the measurement outcome is undertaken by a classical computer (the green box). The unitary evolution on the ancillary system is simulated by a hardware efficient ansatz.

Lemma 5 (Freedom in purification, [25]) *For two purifications $|\phi_1\rangle_{AR}, |\phi_2\rangle_{AR}$ of σ_A on system AR , there exists a unitary transformation U_R such that*

$$|\phi_2\rangle_{AR} = (I_A \otimes U_R)|\phi_1\rangle_{AR}, \quad (14)$$

Based on the fundamental properties of quantum fidelity discussed above, we observe that the following optimization problem characterizes the fidelity function.

Corollary 6 *For any quantum states ρ_A and σ_A on system A , and arbitrary purification $|\psi\rangle_{AR}$ and $|\phi\rangle_{AR}$ of ρ_A and σ_A , it holds that*

$$F(\rho, \sigma) = \max_{U_R} |\langle\psi|_{AR}(I_A \otimes U_R)|\phi\rangle_{AR}|. \quad (15)$$

where the optimization is over any unitaries on system R .

Corollary 6 gives us an elegant variational representation of the fidelity function that only requires purification of input states and optimization over the ancillary system. Following this line of reasoning, we design a variational quantum algorithm to estimate the fidelity of quantum states ρ and σ . We note that in Algorithm 2 the procedure of purifying ρ and σ is realized by VQSL as a subroutine, which will be presented in Sec. III B. Our method formulates the problem of directly calculating the fidelity between two mixed states into an optimization procedure over the ancillary system of two purified states. At the cost of extra subroutines, this approach could deal with arbitrary high-rank states as long as we provide enough ancillary qubits. For numerical performance analysis, we refer to Sec. III C. Besides, we also calculate the analytical gradient of this loss function in Appendix III.

B. Subroutine - quantum state learning and purification

The task of quantum state learning is to find the correct unitary operation such that one could prepare any target mixed

Algorithm 2 Variational Fidelity Estimation (VFE)

Input: quantum states ρ_A and σ_A , circuit ansatz of unitary $U_{AR}(\theta)$, number of iterations ITR;
Output: an estimate of fidelity $F(\rho_A, \sigma_A)$.

Use Purification Subroutine to learn the purified state $|\psi\rangle_{AR}$ of ρ_A and the purified state $|\phi\rangle_{AR}$ of σ_A .
 Initialize parameters θ .
for $itr = 1, \dots, ITR$ **do**
 Apply $U_R(\theta)$ to $|\phi\rangle_{AR}$ and obtain the resulting state $|\tilde{\phi}\rangle_{AR} = I_A \otimes U_R(\theta)|\phi\rangle_{AR}$.
 Compute the loss function $\mathcal{L}_2(\theta) := |\langle\tilde{\phi}|\psi\rangle|_{AR}$.
 Maximize the loss function and update parameters θ ;
end for
 Output the optimized \mathcal{L}_2 as the final fidelity estimation;

state ρ from an initialized state (usually $|0\rangle\langle 0|$ on each qubit). In Ref. [45], the method of state learning for a pure state ρ , where $\text{Rank}(\rho) = 1$, is proposed. Our approach further generalizes it to work for a mixed state ρ , where $\text{Rank}(\rho) \geq 1$. In order to implement our algorithm in NISQ devices, we consider quantum state learning via PQC and the framework of variational quantum algorithms (VQA). The main issue is how to design a faithful loss function \mathcal{L}_3 to guide the learning direction. Such a loss function should be able to quantify the closeness between target ρ and prepared state χ . For pure state cases, simply maximize the state overlap $\text{Tr } \rho \chi$ could help us learn the target state. But for general mixed states, this is not the case. Consider a counter example of $\rho = I/2$ and χ being a random one-qubit mixed state. The overlap is always $\text{Tr } \rho \chi = 1/2$ but this is clearly not the correct distance measure between ρ and χ . On the other hand, the Hilbert-Schmidt norm defined as follows could be a good candidate:

$$\Delta(\rho, \chi) := \|\rho - \chi\|_2^2 = \text{Tr}(\rho - \chi)^2. \quad (16)$$

As the unknown state ρ is fixed, we have

$$\begin{aligned} & \text{argmin}_{\chi} \Delta(\rho, \chi) \\ &= \text{argmin}_{\chi} \text{Tr } \rho^2 + \text{Tr } \chi^2 - 2 \text{Tr } \rho \chi \\ &= \text{argmin}_{\chi} \text{Tr } \chi^2 - 2 \text{Tr } \rho \chi, \end{aligned} \quad (17)$$

where $0 < \text{Tr } \rho^2 < 1$ for mixed state ρ is a constant and hence doesn't influence the optimization direction. Therefore, we choose our loss function to be

$$\min_{\theta} \mathcal{L}_3(\theta) := \text{Tr } \chi^2 - 2 \text{Tr } \rho \chi. \quad (18)$$

Note that this loss function can be implemented on near-term devices since the state overlap can be computed via the Swap test [46, 47]. As a brief reminder, the Swap test evaluates the overlap of two arbitrary states by a single qubit measurement after a combination of Hadamard gates and controlled-swap gates. Evidence has been found that the Swap test has a simple physical implementation in quantum optics [48, 49] and can be experimentally implemented on near-term quantum hardware [50–52].

After discussing the general picture of state learning, we introduce its application in learning the purification of quantum state ρ_A on system A . This can be done by providing an ancillary qubit system R with dimension d_R and initializing the complete system with $|\chi_0\rangle = |00\rangle_{AR}$. Then we apply a parametrized unitary operation $U_{AR}(\theta)$ to drive the system and use classical optimization methods to minimize Eq.(18). In the case of learning purification, we need to set

$$\chi = \text{Tr}_R [U_{AR}(\theta)|\chi_0\rangle\langle\chi_0|U_{AR}^\dagger(\theta)], \quad (19)$$

where the symbol Tr_R denotes the partial trace operation with respect to the ancillary system R . With the above set up, we introduce a variational quantum algorithm to learn the purification of a quantum state ρ_A as follows.

Algorithm 3 Variational Quantum State Learning (VQSL)

Input: quantum states ρ_A , circuit ansatz of unitary $U_{AR}(\theta)$, number of iterations ITR;
Output: a purification of ρ_A .
 Initialize parameters θ .
for $itr = 1, \dots, ITR$ **do**
 Apply $U_{AR}(\theta)$ to three equivalent initial states $|\chi_0\rangle$ on system AR and obtain the resulting partial states: $\chi_A^1 = \chi_A^2 = \chi_A^3 = \text{Tr}_R [U_{AR}(\theta)|\chi_0\rangle\langle\chi_0|U_{AR}^\dagger(\theta)]$;
 Measure the overlap $\langle O \rangle_1 = \text{Tr}(\chi_A^2 \chi_A^3)$ via Swap Test;
 Measure the overlap $\langle O \rangle_2 = \text{Tr}(\rho_A \chi_A^1)$ via Swap Test;
 Compute the loss function $\mathcal{L}_3(\theta) = \langle O \rangle_1 - 2\langle O \rangle_2$;
 Perform optimization for $\mathcal{L}_3(\theta)$ and update parameters θ ;
end for
 Output the final purified state $|\psi\rangle_{AR} = U(\theta^*)|00\rangle_{AR}$;

We want to emphasize that the scope of state learning is much broader than the purification learning task. One could further develop this approach for quantum state preparation and many other applications. For our purpose, learning a purified state to estimate the fidelity is enough. At the cost of introducing ancillary qubits, one could prepare a purification $|\psi\rangle_{AR}$ of target mixed state ρ_A with high fidelity. Then, it will be important to study the performance of VQSL with different ancillary dimensions d_R . The following analysis suggests that only a few ancillary qubits are necessary for low-rank states. For best performance, one should choose the dimension of the ancillary system to be the same as the original system A such that $d_R = d_A$.

Proposition 7 Suppose the input state ρ_A has the spectral decomposition $\rho_A = \sum_{j=1}^k \lambda_j |\psi_j\rangle\langle\psi_j|$ with decreasing spectrum $\{\lambda_j\}_{j=1}^k$. There exists a quantum circuit U_{AR} that approximates the target state ρ_A from $|00\rangle_{AR}$ with a fidelity that satisfies

$$F(\rho_A, \chi_A) = \begin{cases} 1 & \text{if } k \leq d_R, \\ \sqrt{\sum_{j=1}^{d_R} \lambda_j} & \text{otherwise,} \end{cases} \quad (20)$$

where the second case is at least $\sqrt{d_R/k}$.

Proof Assume $d_R \leq d_A$. the goal is to solve

$$\max_{U_{AR}} F(\rho_A, \chi_A), \quad (21)$$

where $\chi_A = \text{Tr}_R [U_{AR}|00\rangle\langle 00|_{AR}U_{AR}^\dagger]$. For convenience, denote the state $U_{AR}|00\rangle_{AR}$ by $|\psi\rangle$ and hence

$$\chi_A = \text{Tr}_R |\psi\rangle\langle\psi|_{AR}. \quad (22)$$

Since the Schmidt rank of $|\psi\rangle$ is at most d_R , the rank of χ_A is also at most d_R .

If $k \leq d_R$, one could choose unitary U_{AR} such that $|\psi\rangle = U_{AR}|00\rangle_{AR} = \sum_{j=1}^k \sqrt{\lambda_j} |\psi_j\rangle_A |\varphi_j\rangle_R$, where $\{|\psi_j\rangle_A\}$ and $\{|\varphi_j\rangle_R\}$ are orthonormal state sets. This ensures that $\chi_A = \text{Tr}_R |\psi\rangle\langle\psi| = \sum_j \lambda_j |\psi_j\rangle\langle\psi_j| = \rho_A$ and leads to a fidelity $F(\rho_A, \chi_A) = 1$. On the other hand, if $k > d_R$, there exists an unitary U such that $|\psi\rangle = U_{AR}|00\rangle_{AR} = \sum_{j=1}^{d_R} \sqrt{\xi_j} |\psi_j\rangle_A |\varphi_j\rangle_R$. In particular, one could further choose $\xi_j = \frac{\lambda_j}{\eta}$ for $j = 1, \dots, d_R$, where the denominator is defined as $\eta = \sum_{\ell=1}^{d_R} \lambda_\ell$. Then, one can calculate the fidelity F as

$$\begin{aligned} F(\rho_A, \chi_A) &= \text{Tr} \sqrt{\chi_A^{1/2} \rho_A \chi_A^{1/2}} \\ &= \sum_{j=1}^{d_R} \sqrt{\lambda_j^2 / \eta} \\ &= \sum_{j=1}^{d_R} \lambda_j / \sqrt{\eta} \\ &= \sqrt{\eta} \geq \sqrt{\frac{d_R}{k}}. \end{aligned} \quad (23)$$

■

C. Numerical experiments

In this section, we conduct numerical experiments to investigate the performance of VFE for state fidelity estimation and its subroutine VQSL for purification learning. The parametrized quantum circuit $U_{AR}(\theta)$ used for Algorithm 3 VQSL and $U_R(\theta)$ for Algorithm 2 are both included in Appendix IV.

We firstly generate 10 random pairs of full-rank density matrices $\{\rho_A^{(1)}, \sigma_A^{(1)} | \dots | \rho_A^{(10)}, \sigma_A^{(10)}\}$ for $n_A = \{1, 2, 3\}$ and calculate the deviation ΔF between the target fidelity and estimated fidelity. As mentioned above, we choose $d_R = d_A$ for best performance in purification learning. The results are summarized in Table. II. The average error rate can be reduced to the level of $< 0.5\%$.

Next, we conduct simulations to qualitatively study the influence of limited ancillary qubits given high-rank states $k > d_R$. 3 random pairs of density matrices, $\{\rho_A^{(1)}, \sigma_A^{(1)} | \rho_A^{(2)}, \sigma_A^{(2)} | \rho_A^{(3)}, \sigma_A^{(3)}\}$, are prepared with $\text{Rank} = \{2, 4, 8\}$ respectively. Then, we test the performance of VFE with different number of ancillary qubits $n_R = \{1, 2, 3\}$. The

Qubit number #	$n_A = 1$	$n_A = 2$	$n_A = 3$
Average error rate $\mathbb{E}[\Delta F]$	0.1694%	0.2476%	0.1960%
Standard deviation $\sigma[\Delta F]$	0.1594%	0.1457%	0.1388%

TABLE II: Error analysis for fidelity estimation VFE between randomly generated full-rank density operators. For purification learning, the Adam optimizer [53] is adopted and hyper-parameters are taken to be depth $L = 6$, learning rate $\text{LR} = 0.2$, and iteration loops $\text{ITR} = 100$ (the latter two parameters are same for VFE). The maximum average error $\mathbb{E}_{\max}[\Delta F] \approx 0.2476\%$ happens at $n_A = 2$, and no clear scaling phenomenon of average error is observed.

results are summarized in Fig. 5. As one can see, the quality of purification learning is directly influenced by the number of ancillary qubits. This limitation could eventually block us from accurately estimate the fidelity between any two high-rank density matrices. This is consistent with the theoretical analysis in Sec. III B.

Here we discuss the trainability issues for VFE and possible solutions. If the best performance of purification of a full-rank state is considered, the number of qubits will be doubled. With an extended system dimension introduced by the purification, VFE might exhibit a barren plateau [35] due to the global loss function defined. This would result an exponentially suppressed gradient with respect to the problem dimension, a phenomenon known as the barren plateau (BP). Ref. [54] shows BP is independent of the optimization methods, meaning that simply change into a gradient-free optimizer would not help. In order to mitigate this trainability issue, several approaches have been proposed such as the parameter initialization and correlation strategies [55, 56], layer-wise learning [57], and variable structure ansatzes [58–60]. We leave the adaptation of these strategies to our VFE for future study.

D. Implementation on superconducting quantum processor

We also apply our VFE to estimate the fidelity between states which are $|+\rangle$ states affected by dephasing channel Deph_p with different intensity p . The result with comparison to the values achieved from simulation are listed in Table III. The experiments are performed on the *IBM quantum* platform, loading the quantum device *ibmq-quito* containing 5 qubits.

Backends	mean	variance	error rate
Theoretical value	0.70710	-	-
Simulator	0.70721	0.00002	0.016%
<i>ibmq-quito</i>	0.71692	0.00003	1.388%

TABLE III: Error analysis for VFE between $\rho = \text{Deph}_{p_1}(|+\rangle)$ and $\sigma = \text{Deph}_{p_2}(|+\rangle)$. We choose $p_1 = 0.2$ and $p_2 = 0.9$, and repeat the experiment 10 times independently.

The input state we choose here are $\rho = \text{Deph}_{p_1}(|+\rangle)$ and $\sigma = \text{Deph}_{p_2}(|+\rangle)$, where $p_1 = 0.2$ and $p_2 = 0.9$. On the quantum device, the input states are prepared similarly to the preparation in Sec. IID and we keep the ancilla as a purification. Next, we operate parameterized quantum circuit on the

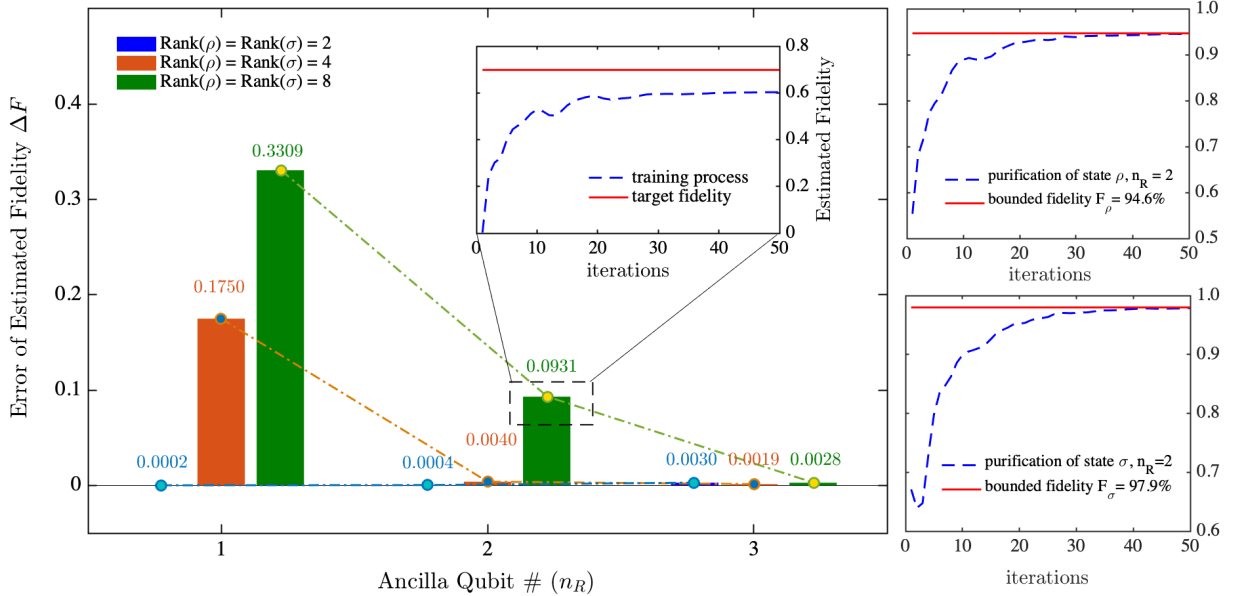


FIG. 5: Performance of VFE given two randomly generated 3-qubit mixed states ρ, σ with different number of ancilla qubits. By providing enough ancilla qubits $n_R = 3$, VFE could estimate the fidelity between two arbitrary full rank mixed states. If not, the purification subroutine will be restricted to produce pure states with fidelity bounded by Eq. (20). This is consistent with the numerical simulation. For the full rank $\text{Rank}(\rho) = 8$ case, given two ancilla qubits $n_R = 2$ to find the purification subroutine is restricted by $F_\rho = \sqrt{\sum_{j=1}^4 \lambda_j(\rho)}$ (shown in subplots on the right column) and the final estimated fidelity will deviate from the target value by $\Delta F \approx 9.31\%$ in this specific case study.

ancilla, and use sequential minimal optimization [44] to optimize the parameters until the loss function converges to its maximum. We repeat 10 independent experiments with same input states and randomly initialized parameters. As demonstrated in Table III, the estimated fidelity from our method are close to the ideal value with stable performance due to a very small variance.

IV. CONCLUSION AND OUTLOOK

In this work, we have introduced near-term quantum algorithms VTDE and VFE to estimate trace distance and quantum fidelity. A strength of our algorithms is that they estimate the metrics directly rather than estimating their bounds. Our algorithms also do not require any assumption on the unknown input states. These algorithms are executable on near-term quantum devices equipped with parameterized quantum circuits. In particular, VTDE could be easily generalized for trace norm estimation for any Hermitian matrix and could avoid the barren plateau issue with logarithmic depth parameterized circuits.

Beyond benchmarking the quantum algorithms' behavior,

our VTDE and VFE could have a wide range of applications in quantum information processing. A direct extension of VTDE might be the estimation for the diamond norm [61–63], which is a widely-used distance measure for quantum channels. The trace distance can also be applied to quantify the Bell non-locality [64], quantum entanglement [65], and the security of quantum cryptography protocols [66], where VTDE could be utilized as a practical subroutine. VFE may be applied to evaluate the conditional quantum mutual information of tripartite quantum states [67]. It is also of great interest to have a further study on the estimation of sandwiched/Geometric Rényi relative entropies [68–70] as an extension of VFE. Efficient estimations of these distance measures could be used to further evaluate the resource measures of entanglement, coherence, magic and other resources in quantum information [71–82].

Acknowledgements.

We thank Runyao Duan, Yuao Chen, and Mark M. Wilde for helpful discussions. R. C. and Z. S. contributed equally to this work. This work was done when R. C., Z. S., and X. Z. were research interns at Baidu Research.

[1] J. Preskill, *Quantum* **2**, 79 (2018), arXiv:1801.00862 .
[2] J. R. McClean, J. Romero, R. Babbush, and A. Aspuru-Guzik, *New Journal of Physics* **18**, 023023 (2016), arXiv:1509.04279 .
[3] J. Biamonte, P. Wittek, N. Pancotti, P. Rebentrost, N. Wiebe, and S. Lloyd, *Nature* **549**, 195 (2017).
[4] M. Schuld, I. Sinayskiy, and F. Petruccione, *Contemporary*

Physics **56**, 172 (2015).

[5] S. Arunachalam and R. de Wolf, *ACM SIGACT News* **48**, 41 (2017), [arXiv:1701.06806](https://arxiv.org/abs/1701.06806).

[6] M. Benedetti, E. Lloyd, S. Sack, and M. Fiorentini, *Quantum Science and Technology* **4**, 043001 (2019), [arXiv:1906.07682](https://arxiv.org/abs/1906.07682).

[7] A. Peruzzo, J. McClean, P. Shadbolt, M.-H. Yung, X.-Q. Zhou, P. J. Love, A. Aspuru-Guzik, and J. L. O’Brien, *Nature Communications* **5**, 4213 (2014), [arXiv:1304.3061](https://arxiv.org/abs/1304.3061).

[8] K. M. Nakanishi, K. Mitarai, and K. Fujii, *Physical Review Research* **1**, 033062 (2019).

[9] K. Sharma, M. Cerezo, L. Cincio, and P. J. Coles, [arXiv:2005.12458](https://arxiv.org/abs/2005.12458) (2020), [arXiv:2005.12458](https://arxiv.org/abs/2005.12458).

[10] X. Yuan, S. Endo, Q. Zhao, Y. Li, and S. C. Benjamin, *Quantum* **3**, 191 (2019), [arXiv:1812.08767](https://arxiv.org/abs/1812.08767).

[11] J. Wu and T. H. Hsieh, *Physical Review Letters* **123**, 220502 (2019), [arXiv:1811.11756](https://arxiv.org/abs/1811.11756).

[12] Y. Wang, G. Li, and X. Wang, [arXiv:2005.08797](https://arxiv.org/abs/2005.08797) (2020), [arXiv:2005.08797](https://arxiv.org/abs/2005.08797).

[13] A. N. Chowdhury, G. H. Low, and N. Wiebe, , 1 (2020), [arXiv:2002.00055](https://arxiv.org/abs/2002.00055).

[14] X. Xu, J. Sun, S. Endo, Y. Li, S. C. Benjamin, and X. Yuan, *arXiv preprint arXiv:1909.03898* **2**, 1 (2019), [arXiv:1909.03898](https://arxiv.org/abs/1909.03898).

[15] C. Bravo-Prieto, R. LaRose, M. Cerezo, Y. Subasi, L. Cincio, and P. J. Coles, [arXiv:1909.05820](https://arxiv.org/abs/1909.05820) (2019), [arXiv:1909.05820](https://arxiv.org/abs/1909.05820).

[16] H.-Y. Huang, K. Bharti, and P. Rebentrost, [arXiv:1909.07344](https://arxiv.org/abs/1909.07344) (2019), [arXiv:1909.07344](https://arxiv.org/abs/1909.07344).

[17] X. Wang, Z. Song, and Y. Wang, [arXiv:2006.02336](https://arxiv.org/abs/2006.02336) (2020), [arXiv:2006.02336](https://arxiv.org/abs/2006.02336).

[18] C. Bravo-Prieto, D. Garcia-Martin, and J. I. Latorre, *Physical Review A* **101**, 062310 (2020), [arXiv:1905.01353](https://arxiv.org/abs/1905.01353).

[19] S. Endo, Z. Cai, S. C. Benjamin, and X. Yuan, [arXiv:2011.01382](https://arxiv.org/abs/2011.01382), 1 (2020), [arXiv:2011.01382](https://arxiv.org/abs/2011.01382).

[20] M. Cerezo, A. Arrasmith, R. Babbush, S. C. Benjamin, S. Endo, K. Fujii, J. R. McClean, K. Mitarai, X. Yuan, L. Cincio, *et al.*, *Nature Reviews Physics*, 1 (2021).

[21] K. Bharti, A. Cervera-Lierta, T. H. Kyaw, T. Haug, S. Alperin-Lea, A. Anand, M. Degroote, H. Heimonen, J. S. Kottmann, T. Menke, *et al.*, *arXiv preprint arXiv:2101.08448* (2021).

[22] B. M. Terhal, *Reviews of Modern Physics* **87**, 307 (2015), [arXiv:arXiv:1302.3428v1](https://arxiv.org/abs/1302.3428v1).

[23] L. Hu, S.-H. Wu, W. Cai, Y. Ma, X. Mu, Y. Xu, H. Wang, Y. Song, D.-L. Deng, C.-L. Zou, and et al., *Science Advances* **5**, eaav2761 (2019).

[24] P. Braccia, F. Caruso, and L. Banchi, “How to enhance quantum generative adversarial learning of noisy information,” *arXiv preprint arXiv: 2012.05996* (2020).

[25] M. A. Nielsen and I. L. Chuang, *Quantum computation and quantum information* (Cambridge university press, 2010).

[26] R. Jozsa, *Journal of Modern Optics* **41**, 2315 (1994).

[27] A. Uhlmann, *Reports on Mathematical Physics* **9**, 273 (1976).

[28] H. Buhrman, R. Cleve, J. Watrous, and R. de Wolf, *Physical Review Letters* **87** (2001), 10.1103/physrevlett.87.167902.

[29] J. Watrous, “Quantum computational complexity,” (2008), [arXiv:0804.3401 \[quant-ph\]](https://arxiv.org/abs/0804.3401).

[30] M. Cerezo, A. Poremba, L. Cincio, and P. J. Coles, *Quantum* **4**, 248 (2020), [arXiv:1906.09253](https://arxiv.org/abs/1906.09253).

[31] J. Zhang, P. Ruggiero, and P. Calabrese, *Physical Review Letters* **122** (2019), 10.1103/physrevlett.122.141602.

[32] A. Smirne, D. Brivio, S. Cialdi, B. Vacchini, and M. G. A. Paris, *Physical Review A* **84** (2011), 10.1103/physreva.84.032112.

[33] A. Kandala, A. Mezzacapo, K. Temme, M. Takita, M. Brink, J. M. Chow, and J. M. Gambetta, *Nature* **549**, 242–246 (2017).

[34] B. Commeau, M. Cerezo, Z. Holmes, L. Cincio, P. J. Coles, and A. Sornborger, “Variational hamiltonian diagonalization for dynamical quantum simulation,” (2020), [arXiv:2009.02559 \[quant-ph\]](https://arxiv.org/abs/2009.02559).

[35] J. R. McClean, S. Boixo, V. N. Smelyanskiy, R. Babbush, and H. Neven, *Nature communications* **9**, 1 (2018).

[36] K. Mitarai, M. Negoro, M. Kitagawa, and K. Fujii, *Phys. Rev. A* **98**, 032309 (2018).

[37] M. Schuld, V. Bergholm, C. Gogolin, J. Izaac, and N. Killoran, *Phys. Rev. A* **99**, 032331 (2019).

[38] M. Cerezo, A. Sone, T. Volkoff, L. Cincio, and P. J. Coles, [arXiv:2001.00550](https://arxiv.org/abs/2001.00550) (2020), [arXiv:2001.00550](https://arxiv.org/abs/2001.00550).

[39] M. M. Wilde, *Proceedings of the Royal Society A: Mathematical, Physical and Engineering Sciences* **469**, 20130259 (2013).

[40] “Paddle Quantum,” (2020).

[41] <https://github.com/paddlepaddle/paddle>.

[42] Y. Ma, D. Yu, T. Wu, and H. Wang, *Frontiers of Data and Domputing* **1**, 105 (2019).

[43] S. Sim, P. D. Johnson, and A. Aspuru-Guzik, *Advanced Quantum Technologies* **2**, 1900070 (2019).

[44] K. M. Nakanishi, K. Fujii, and S. Todo, *Phys. Rev. Research* **2**, 043158 (2020).

[45] S. M. Lee, J. Lee, and J. Bang, *Physical Review A* **98**, 052302 (2018).

[46] H. Buhrman, R. Cleve, J. Watrous, and R. de Wolf, *Physical Review Letters* **87**, 167902 (2001), [arXiv:0102001 \[quant-ph\]](https://arxiv.org/abs/0102001).

[47] D. Gottesman and I. Chuang, [arXiv:quant-ph/0105032](https://arxiv.org/abs/quant-ph/0105032) (2001), [arXiv:0105032 \[quant-ph\]](https://arxiv.org/abs/0105032).

[48] A. K. Ekert, C. M. Alves, D. K. L. Oi, M. Horodecki, P. Horodecki, and L. C. Kwek, *Physical review letters* **88**, 217901 (2002).

[49] J. C. Garcia-Escartin and P. Chamorro-Posada, *Physical Review A* **87**, 052330 (2013), [arXiv:1303.6814](https://arxiv.org/abs/1303.6814).

[50] R. Islam, R. Ma, P. M. Preiss, M. Eric Tai, A. Lukin, M. Rispoli, and M. Greiner, *Nature* **528**, 77 (2015).

[51] R. B. Patel, J. Ho, F. Ferreyrol, T. C. Ralph, and G. J. Pryde, *Science advances* **2**, e1501531 (2016).

[52] N. M. Linke, S. Johri, C. Figgatt, K. A. Landsman, A. Y. Matsuda, and C. Monroe, *Physical Review A* **98**, 052334 (2018).

[53] D. P. Kingma and J. Ba, *arXiv preprint arXiv:1412.6980* (2014).

[54] A. Arrasmith, M. Cerezo, P. Czarnik, L. Cincio, and P. J. Coles, *arXiv preprint arXiv:2011.12245* (2020).

[55] E. Grant, L. Wossnig, M. Ostaszewski, and M. Benedetti, *Quantum* **3**, 214 (2019).

[56] T. Volkoff and P. J. Coles, *Quantum Science and Technology* **6**, 025008 (2021).

[57] A. Skolik, J. R. McClean, M. Mohseni, P. van der Smagt, and M. Leib, “Layerwise learning for quantum neural networks,” (2020), [arXiv:2006.14904 \[quant-ph\]](https://arxiv.org/abs/2006.14904).

[58] H. R. Grimsley, S. E. Economou, E. Barnes, and N. J. Mayhall, *Nature communications* **10**, 1 (2019).

[59] A. G. Rattew, S. Hu, M. Pistoia, R. Chen, and S. Wood, *arXiv preprint arXiv:1910.09694* (2019).

[60] M. Bilkis, M. Cerezo, G. Verdon, P. J. Coles, and L. Cincio, *arXiv preprint arXiv:2103.06712* (2021).

[61] A. Kitaev and J. Watrous, in *Proceedings of the thirty-second annual ACM symposium on Theory of computing - STOC '00* (ACM Press, New York, New York, USA, 2000) pp. 608–617.

[62] J. Watrous, *Theory of Computing* **5**, 217 (2009).

[63] J. Watrous, “Simpler semidefinite programs for completely bounded norms,” (2012), [arXiv:1207.5726 \[quant-ph\]](https://arxiv.org/abs/1207.5726).

[64] S. G. A. Brito, B. Amaral, and R. Chaves, *Physical Review A* **97** (2018), 10.1103/physreva.97.022111.

[65] G. Vidal and R. F. Werner, *Phys. Rev. A* **65**, 032314 (2002).

[66] H. Yuen, “What the trace distance security criterion in quantum key distribution does and does not guarantee,” (2014), [arXiv:1410.6945 \[quant-ph\]](https://arxiv.org/abs/1410.6945) .

[67] M. Berta and M. Tomamichel, *IEEE Transactions on Information Theory* **62**, 1758–1763 (2016).

[68] M. Müller-Lennert, F. Dupuis, O. Szehr, S. Fehr, and M. Tomamichel, *Journal of Mathematical Physics* **54**, 122203 (2013), [arXiv:1306.3142](https://arxiv.org/abs/1306.3142) .

[69] M. M. Wilde, A. Winter, and D. Yang, *Communications in Mathematical Physics* **331**, 593 (2014).

[70] K. Matsumoto, Reality and Measurement in Algebraic Quantum Theory , 229 (2018).

[71] E. Chitambar and G. Gour, *Reviews of Modern Physics* **91**, 025001 (2019), [arXiv:1806.06107](https://arxiv.org/abs/1806.06107) .

[72] M. B. Plenio and S. S. Virmani, *Quantum Information and Computation* **7**, 1 (2007).

[73] X. Wang and R. Duan, *Physical Review Letters* **119**, 180506 (2017), [arXiv:1606.09421](https://arxiv.org/abs/1606.09421) .

[74] V. Vedral, *Reviews of Modern Physics* **74**, 197 (2002).

[75] X. Wang and M. M. Wilde, *Physical Review Letters* **125**, 040502 (2020), [arXiv:2007.14270](https://arxiv.org/abs/2007.14270) .

[76] N. Datta, *IEEE Transactions on Information Theory* **55**, 2816 (2009).

[77] K. Wang, X. Wang, and M. M. Wilde, [arXiv:1911.07433](https://arxiv.org/abs/1911.07433)

Supplemental Material of Variational Quantum Metric Estimation

I. DETAILED PROOFS

A. Proof of Proposition 1

Proposition 1 For any Hermitian matrix $H_{AB} \in \mathcal{L}(\mathcal{H}_A \otimes \mathcal{H}_B)$ with spectral decomposition as Eq. (3), respectively denote the dimension of \mathcal{H}_A , \mathcal{H}_B by d_A , d_B . It holds that

$$\max_U \text{Tr} |0\rangle\langle 0|_A \tilde{H}_A = \sum_{j=1}^{d_B} h_{AB}^j, \quad (\text{S1})$$

where $\tilde{H}_A = \text{Tr}_B \tilde{H}_{AB}$, $\tilde{H}_{AB} = U H_{AB} U^\dagger$, and the optimization is over all unitaries.

Proof By the definition of partial trace, we have

$$\begin{aligned} \text{Tr} |0\rangle\langle 0|_A \tilde{H}_A &= \text{Tr} |0\rangle\langle 0|_A \otimes I_B \tilde{H}_{AB} \\ &= \sum_{j=1}^{d_B} \tilde{H}_{AB}^{j,j}, \end{aligned} \quad (\text{S2})$$

where $\tilde{H}_{AB}^{j,j}$ is the j -th diagonal element of the matrix representation of \tilde{H}_{AB} . Since H_{AB} and \tilde{H}_{AB} have the same decreasing spectrum $\{h_{AB}^j\}_{j=1}^{d_A d_B}$, which majorizes the diagonal elements of \tilde{H}_{AB} [83, p. 254, Theorem 4.3.50], we have

$$\begin{aligned} \text{Tr} |0\rangle\langle 0|_A \tilde{H}_A &= \sum_{k=1}^{d_B} \tilde{H}_{AB}^{k,k} \\ &\leq \sum_{j=1}^{d_B} h_{AB}^j. \end{aligned} \quad (\text{S3})$$

As the equality of Eq. S3 holds when \tilde{H}_{AB} is diagonalized under the computational basis, the proof is complete. \blacksquare

B. Proof of Theorem 2

Theorem 2 For any Hermitian H_A on n -qubit system A , and any single-qubit pure state $|r\rangle$ on system R , it holds that

$$\|H_A\|_1 = \max_{U^+} \text{Tr} |0\rangle\langle 0|_R Q_R^+ + \max_{U^-} \text{Tr} |0\rangle\langle 0|_R Q_R^-, \quad (\text{S4})$$

where $Q_R^\pm = \text{Tr}_A Q_{AR}^\pm$, $Q_{AR}^\pm = U^\pm(\pm H_A \otimes |r\rangle\langle r|_R)U^{\pm\dagger}$, and each optimization is over unitaries on system AR .

Proof The trace norm $\|H_A\|_1$ equals to the sum of the absolute values of H_A 's eigenvalues:

$$\|H_A\|_1 = \sum_{j=1}^{d_A} |h_A^j| = \sum_{h_A^j > 0} h_A^j + \sum_{h_A^j < 0} -h_A^j. \quad (\text{S5})$$

Observe that H_A and $H_A \otimes |r\rangle\langle r|_R$ have the same spectrum, up to d_A 0 eigenvalues. Denote the decreasing spectrum of $H_A \otimes |r\rangle\langle r|_R$ by $\{h_{AR}^j\}_{j=1}^{2d_A}$. Then this observation implies that

$$\sum_{j=1}^{d_A} h_{AR}^j = \sum_{h_A^j > 0} h_A^j, \quad \sum_{j=d_A+1}^{2d_A} h_{AR}^j = \sum_{h_A^j < 0} -h_A^j. \quad (\text{S6})$$

According to Proposition 1, for $Q_{AR}^+ = U^+(H_A \otimes |r\rangle\langle r|_R)U^{+\dagger}$, $\max_{U^+} \text{Tr} |r\rangle\langle r|_R Q_R^+$ equals to the sum of the first half eigenvalues of $H_A \otimes |r\rangle\langle r|_R$:

$$\max_{U^+} \text{Tr} |0\rangle\langle 0|_R Q_R^+ = \sum_{j=1}^{d_A} h_{AR}^j. \quad (\text{S7})$$

Similarly, for $Q_{AR}^- = U^-(-H_A \otimes |r\rangle\langle r|_R)U^{-\dagger}$, $\max_{U^-} \text{Tr} |r\rangle\langle r|_R Q_R^-$ equals to the sum of the first half eigenvalues of $-H_A \otimes |r\rangle\langle r|_R$, or to say, the sum of the absolute value of the last half eigenvalues of $H_A \otimes |r\rangle\langle r|_R$:

$$\max_{U^-} \text{Tr} |0\rangle\langle 0|_R Q_R^- = \sum_{j=d_A+1}^{2d_A} -h_{AR}^j = \sum_{j=d_A+1}^{2d_A} |h_{AR}^j|. \quad (\text{S8})$$

Together with Eq. S5, S6, S7, S8 we have

$$\|H_A\|_1 = \max_{U^+} \text{Tr} |0\rangle\langle 0|_R Q_R^+ + \max_{U^-} \text{Tr} |0\rangle\langle 0|_R Q_R^-, \quad (\text{S9})$$

which completes the proof. \blacksquare

II. A NAIVE ALGORITHM FOR TRACE DISTANCE ESTIMATION

From the definition of trace norm, one may naturally try to learn $\|H\|_1$ by twice optimizing over projectors. Explicitly, we have the following proposition:

Proposition S1 The trace norm $\|H\|_1$ can be obtained by:

$$\|H\|_1 = \max_{P_+} \text{Tr}(P_+ H) + \max_{P_-} \text{Tr}(-P_- H), \quad (\text{S10})$$

where each optimization is over projectors. The optimized projector P_\pm is rank- k_\pm , where k_\pm is the number of the positive/negative eigenvalues of H .

Proof Consider the spectrum decomposition of H :

$$\begin{aligned} H &= \sum_{j=1}^d h^j |\psi_j\rangle\langle\psi_j| \\ &= \sum_{h^j > 0} h^j |\psi_j\rangle\langle\psi_j| + \sum_{h^j < 0} h^j |\psi_j\rangle\langle\psi_j| \end{aligned} \quad (\text{S11})$$

where d is the dimension of H . Let

$$S = \sum_{h^j > 0} h^j |\psi_j\rangle\langle\psi_j|, \quad T = - \sum_{h^j < 0} h^j |\psi_j\rangle\langle\psi_j|$$

so that

$$H = S - T, \quad \|H\|_1 = \text{Tr } S + \text{Tr } T, \quad (\text{S12})$$

and S and T are positive and orthogonal. In this sense, we have

$$\begin{aligned} \text{Tr}(P_+ H) &= \text{Tr}(P_+(S - T)) \leq \text{Tr}(P_+ S) \leq \text{Tr } S \\ \text{Tr}(-P_- H) &= \text{Tr}(P_-(T - S)) \leq \text{Tr}(P_- T) \leq \text{Tr } T \end{aligned} \quad (\text{S13})$$

The two inequalities become equal when P_{\pm} is the projector onto the support of S and T , respectively. Thus the optimized projectors P_{\pm} is rank- k_{\pm} , where k_{\pm} is the rank of S/T , i. e., the number of the positive/negative eigenvalues of H . Eq. S12 and Eq. S13 imply Eq. S10, which finish the proof. ■

Using similar technique in the proof of Corollary 3 we can have following corollary on trace distance estimation from Proposition S1.

Corollary S2 For any quantum states ρ and σ , it holds that

$$D(\rho, \sigma) = \max_P \text{Tr } P(\rho - \sigma), \quad (\text{S14})$$

and the optimized projector P is rank- k , where k is the number of the positive eigenvalues of $\rho - \sigma$.

In practice, any rank- k projector can be characterized by

$$P_{\text{rank-}k} = \sum_{j=1}^k U|j\rangle\langle j|U^\dagger, \quad (\text{S15})$$

and one can obtain $\text{Tr } P_{\text{rank-}k} H = \sum_{j=1}^k \text{Tr } HU|j\rangle\langle j|U^\dagger$.

If one does not have k as prior knowledge of ρ, σ , one has to try different k until $\max_U \text{Tr } P_{\text{rank-}k}(\rho - \sigma)$ reaches a maximum with respect to k . Then one have the following intuitive (but somehow naive) algorithm for trace distance estimation:

Algorithm 4 naive Variational Trace Distance Estimation (nVTDE)

Input: n -qubit quantum states ρ and σ , circuit ansatz of unitary $U_{AR}(\theta)$, number of iterations ITR;

Output: an estimation of $D(\rho, \sigma)$.

for $k = 1, \dots, 2^n - 1$ **do**

 Initialize parameters θ .

for $\text{itr} = 1, \dots, \text{ITR}$ **do**

 Prepare k quantum states $|j\rangle$, $j \in [1, k]$;

 Apply $U(\theta)$ respectively to all $|j\rangle$, and obtain $\mathcal{L}_4^k = \sum_{j=1}^k (\text{Tr } U\rho U^\dagger |j\rangle\langle j| - \text{Tr } U\sigma U^\dagger |j\rangle\langle j|)$;

 Maximize the loss function \mathcal{L}_4^k and update parameters of θ ;

end for

if $\max_{\theta} \mathcal{L}_4^k(\theta)$ does not increase with k **then**

 break

end if

end for

Output \mathcal{L}_4 as the trace distance estimation;

Algorithm 4, though requires no ancillary qubit, is inefficient for a large k . From the perspective of quantum resources, Algorithm 4 needs at least k computational basis quantum states. From the perspective of time, Algorithm 4 also needs k rounds of optimization. In the worst case, $k = 2^n - 1$.

We remark that, if one of the two unknown states is pure (suppose ρ is the pure state), then $\rho - \sigma$ has at most one positive eigenvalue. Explicitly, we have the following lemma:

Lemma S3 *If ρ is a pure state and σ is a mixed state, then $\rho - \sigma$ has at most one positive eigenvalue.*

Proof According to the Weyl's inequality in matrix theory (see [84]), for Hermitian matrices $A, B, C = A + B$, we have

$$c^{j+k-1} \leq a^j + b^k \leq c^{j+k-d}, \quad (\text{S16})$$

where a^j, b^j and c^j are the j -th largest eigenvalue of A, B and C , respectively, and d is the dimension. Let $k = d = 2^n$, $A = \rho - \sigma$, $B = \sigma$ and use the second inequality:

$$a^j + b^d \leq c^j. \quad (\text{S17})$$

We use the fact that σ is positive (which implies $b^d \geq 0$), and $\text{Rank}(\rho) = 1$ (which implies $c^j = 0$ for $j \geq 2$). Finally we have

$$a^j \leq 0, \forall j \geq 2, \quad (\text{S18})$$

which complete the proof that $\rho - \sigma$ has at most one positive eigenvalue. \blacksquare

Thus, if one of the two states is pure, we only have to prepare one rank-1 projector $|0\rangle\langle 0|$.

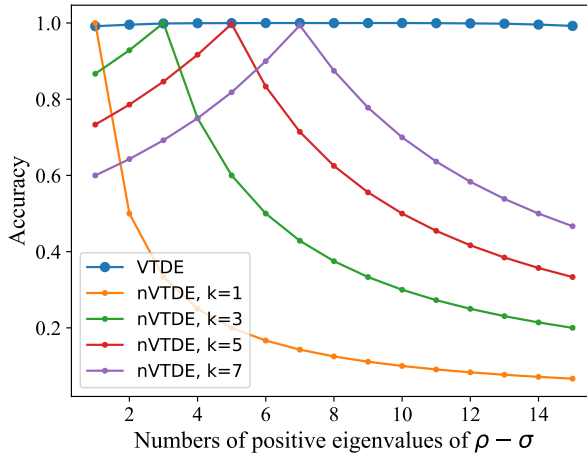


FIG. 6: Trace distance learned by VTDE and nVTDE versus the number of positive eigenvalues of $H = \frac{1}{2}(\rho - \sigma)$. The curves show that the performance of VTDE is stable with different numbers of positive eigenvalues. In contrast, the performance of nVTDE relies heavily on the difference between k and the number of positive eigenvalues.

Fig. 6 shows the behavior of VTDE and nVTDE for $\rho - \sigma$ with different number of positive eigenvalues. In the $n = 4$ case, the number of positive eigenvalues can range from 1 to $2^4 - 1$. Fig. 6 shows that the performance of VTDE is stable with different numbers of positive eigenvalues, while the performance of nVTDE relies heavily on the difference between k and the number of positive eigenvalues, as analyzed above.

III. ANALYTICAL GRADIENT FOR VFE

Recall the loss function for VFE,

$$\mathcal{L}(\boldsymbol{\theta}) = {}_{AR}\langle \psi | I_A \otimes U_R(\boldsymbol{\theta}) | \phi \rangle_{AR}. \quad (\text{S19})$$

Consider the parametrized quantum circuit $U(\boldsymbol{\theta}) = \prod_{i=1}^n U_i(\theta_i)$, where each gate U_i is either fixed, e.g., C-NOT gate, or generated by $U_i = e^{-i\theta_i H_i/2}$. For convenience, denote $U_{i:j} = U_i \cdots U_j$. We can write the cost function as

$$\mathcal{L}(\boldsymbol{\theta}) = {}_{AR}\langle \psi | I_A \otimes U_{1:n}(\theta_{1:n}) | \phi \rangle_{AR}. \quad (\text{S20})$$

Absorb all gates except the one we want to calculate the gradient into $\langle \psi |$ and $|\phi\rangle$:

$$\begin{aligned}\mathcal{L}(\boldsymbol{\theta}) &= {}_{AR}\langle \psi | (I_A \otimes U_1) \cdots (I_A \otimes U_j) \cdots (I_A \otimes U_n) |\phi \rangle_{AR} \\ &= {}_{AR}\langle \psi' | (I_A \otimes U_j) |\phi' \rangle_{AR},\end{aligned}\quad (\text{S21})$$

where $|\phi'\rangle_{AR} = (I_A \otimes U_{j+1:n})|\phi\rangle_{AR}$ and $\langle \psi' |_{AR} = \langle \psi |_{AR}(I_A \otimes U_{1:j-1})$. With the following property,

$$\frac{\partial U_{1:n}}{\partial \theta_j} = -\frac{i}{2} U_{1:j-1} (H_j U_j) U_{j+1:n}, \quad (\text{S22})$$

the gradient is calculated to be

$$\frac{\partial \mathcal{L}(\boldsymbol{\theta})}{\partial \theta_j} = -\frac{i}{2} {}_{AR}\langle \psi' | (I_A \otimes H_j U_j) |\phi' \rangle_{AR}. \quad (\text{S23})$$

We can absorb the Pauli product H_j into U_j by an rotation on $\theta_j \rightarrow \theta_j \pm \pi$:

$$\begin{aligned}U_j(\pm\pi) &= e^{\mp i\pi H_j/2} \\ &= \mp i H_j,\end{aligned}\quad (\text{S24})$$

which leads to

$$\begin{aligned}\frac{\partial \mathcal{L}(\boldsymbol{\theta})}{\partial \theta_j} &= \frac{1}{2} {}_{AR}\langle \psi | (I_B \otimes U_j(\theta_j + \pi)) |\phi \rangle_{AR} \\ &= \frac{1}{2} L(\theta_j + \pi).\end{aligned}\quad (\text{S25})$$

IV. QUANTUM CIRCUIT FOR VFE

There are two types of parametrized quantum circuit used in VFE. The first type $U_R(\boldsymbol{\theta})$ only acts on the ancillary system and aims at fulfilling Algorithm 2. In this specific study, it is taken to be the U_3 rotation gate on Bloch sphere, 2-qubit universal gate [85], and 3-qubit universal gate [86] for $n_A = \{1, 2, 3\}$ respectively. The second type serves for Algorithm 3 purification learning and is shown in Fig. 7.

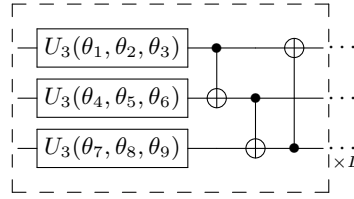


FIG. 7: Parameterized ansatz $U_{AR}(\boldsymbol{\theta})$ used for state learning. Depth L denotes the number of repetitions of the same block (dashed-line box). Each block consists of a column of general $U_3(\theta, \phi, \varphi) = R_z(\phi)R_y(\theta)R_z(\varphi)$ rotations for each qubit, followed with a circular layer of CNOT gates. Notice that the number of parameters in this ansatz increases linearly with the circuit depth L and the number of qubits.